

Tunable wave propagation by varying prestrain in tensegrity-based periodic media

Raj Kumar Pal^a, Massimo Ruzzene^{a,b} and Julian J. Rimoli^a

^a School of Aerospace Engineering, Georgia Institute of Technology, Atlanta GA 30332

^b School of Mechanical Engineering, Georgia Institute of Technology, Atlanta GA 30332

Abstract

This paper investigates the dynamic properties of one, two and three-dimensional tensegrity-based periodic structures introduced in [1], which are here termed as tensegrity beams, plates and solids, respectively. We study their linear wave propagation properties and show that in each case, these properties can be significantly altered by the prestrain in the cables. As the prestrain is varied, we observe jumps in the wave velocities at two critical prestrain values, which define transitions between the three distinct phases of these structural assemblies. At low cable prestrains, the wave speeds are zero as the lattices have zero effective stiffness. At moderate prestrains, the wave speed is nonzero and finally, at prestrain levels where the bars buckle, the wave speed decreases to a lower value. Dispersion analysis on these beams, plates and solids reveal unique properties such as very low wave velocities compared to their constituent material and the existence of flat bands at low frequencies. Furthermore, we find that shear waves travel faster than longitudinal waves in tensegrity solids in a range of cable prestrains. Finally, we verify the key observations through detailed numerical simulations on finite tensegrity solids.

1. Introduction

Artificially engineered lattices have been the subject of extensive research over the past decade due to their unique static and dynamic properties [2, 3]. Examples include pentamode lattices with zero shear modulus [4, 5], auxetic lattices with negative Poisson's ratio [6, 7] and hexagonal lattices featuring frequency bandgaps [8, 9]. These lattices fall under the category of metamaterials and metastructures that have potential for unprecedented control over the effective structural properties through the careful design of their microstructure. In recent years, there has been an increased focus on developing structures and lattices whose mechanical properties can be significantly altered by applying external fields. Examples include elastomers with holes in periodic arrangements [10], deformable hexagonal lattices [11], origami [12] and tensegrity based structures [1, 13], among others.

Tensegrity structures are meta-structures composed of an assembly of prestressed bars and cables, connected in such a way that the cables (bars) are in tension (compression) and the structure is

in equilibrium without any external force [14, 15]. Simple examples of tensegrity structures include an archery bow and the human bone tendon arrangement [16]. Their structural integrity arises as a consequence of the member prestrain. A key property of these structures which makes them distinct from conventional load carrying ones is that their compression carrying members (bars) are isolated while the tensile load carrying members (cables) are all connected. Tensegrity lattices offer unique possibilities for tunable static [1] and dynamic properties [17] by varying the cable prestrain. Potential applications range from deployable structures [16] to robotics [18] and impact mitigation structures [19].

Developing a periodic tensegrity lattice is a non-trivial task since most of the tensegrity structures lack translation symmetry and cannot tessellate a 3D domain. There have been a few notable examples in the past decade for developing tensegrity-based beams and plates [16, 20]. However, these designs have a continuous path of bars spanning the entire structure and do not share the unique topological properties of tensegrity structures like

localized span of compressive elements. Moreover they do not easily extend to 3D tensegrity solids. Recently, Rimoli and Pal [1] developed a unit cell for a 3D periodic tensegrity lattice by exploiting the symmetries of a truncated octahedron tensegrity sphere. This lattice satisfies all the conditions of a tensegrity structure in the sense that only the tensile members are path connected to one another.

In this letter, we investigate the dynamic properties of tensegrity based 1D, 2D and 3D periodic structures introduced in [1], which are here termed as tensegrity beams, plates and solids, respectively. We study their linear wave properties using dispersion analysis and show how these properties can be significantly altered by varying the cable prestrain. We model the bars as elastic or deformable systems in a geometrically nonlinear elasticity framework in contrast to prior investigations [21, 22, 23, 24] that treat the bars and cables as perfectly rigid or implicitly assume that cables (bars) only experience tension (compression). As the prestrain is varied, we observe jumps in wavespeeds at two critical prestrain values and draw parallels with phase transitions in condensed matter systems. Our dispersion analyses also reveal unique properties like faster shear waves than longitudinal waves for a range of cable prestrain in tensegrity solids.

The outline of this letter is as follows: In Sec. 2 we briefly describe the lattice unit cell and our modeling methodology. Section 3 presents dispersion diagrams and wave speeds at low frequencies under a range of cable prestrains, illustrating the unique dynamics of these lattices. Finally, the conclusions are summarized in Sec. 4.

2. Lattice description and modeling approach

The tensegrity structure employed as the building block for the tensegrity beams, plates and solids is described in detail in [1] and depicted in Fig. 1(a). Its nodes lie at the vertices of a truncated octahedron and it comprises of 12 bars (black, dark lines) in the interior and 36 cables (red, light lines) along the edges of the octahedron. The bars and cables intersect at nodes, which are modeled as perfect pin joints. This structure lacks translation symmetry as the two square facets on opposite ends are twisted about their normal axis relative to each other. According to [1], a unit cell with translation symmetry can be obtained by performing a sequence of reflection operations. These operations lead to a unit cell for

a tensegrity beam (periodic along x in Fig. 1(b)), plate (periodic along x and y in Fig. 1(c)) and solid (periodic along x , y and z in Fig. 1(d)), satisfying the required translation symmetries along the lattice vector directions. The tensegrity lattice also has a C_4 rotational symmetry about the axes passing through the center of the unit cell and coinciding with the lattice vector directions \mathbf{a}_k . Note that each unit cell in isolation has C_2 symmetry, while the $\pi/4$ rotational symmetry is obtained by gliding $|\mathbf{a}_k|/2$ along this axis, resulting in an infinite lattice having C_4 symmetry.

A key feature of tensegrity structures is that the level of tension (compression) can be varied by varying the member prestrain, characterized here by a cable prestrain parameter λ . It is defined with respect to our canonical unit cell, which is a purely geometric entity as illustrated in Fig. 1, with the unique property that all bar (cable) lengths are equal. λ is the ratio of the undeformed cable length to the length of the cable segment in this canonical unit cell. We assume here that all the cables have identical prestrain parameter λ and that the bar lengths are identical to that in the canonical unit cell. When the bars and cables (with $\lambda < 1$) are assembled, the cables get stretched and the bars get compressed until an equilibrium configuration is reached. This equilibrium configuration is determined by using a Newton-Raphson procedure [25, 1] and is taken to be the reference configuration for the lattice. As λ varies, the reference configuration thus changes. The dispersion and wave propagation analyses are conducted on this reference configuration. The lattice vectors in each periodic direction are determined by the difference of position vectors between the corresponding nodes on opposite square facets in Fig. 1. Since the cable prestrains are equal, the lattice vectors are of equal magnitude and are orthogonal due to symmetry.

The bars and cables are modeled as beams made of linear elastic materials, capable of undergoing large deformations. We use an equivalent spring mass model for each beam, where the spring stiffness and masses are chosen to match the axial stiffness, total mass and mass moment of inertia, and buckling load of the continuum beam. Each beam comprises of 4 point masses, with each mass having three translational degrees of freedom. The mass at each node is simply the sum of the end mass of all the bars and cables meeting there. Details of the model are presented in [19].

To analyze the linear wave propagation response,

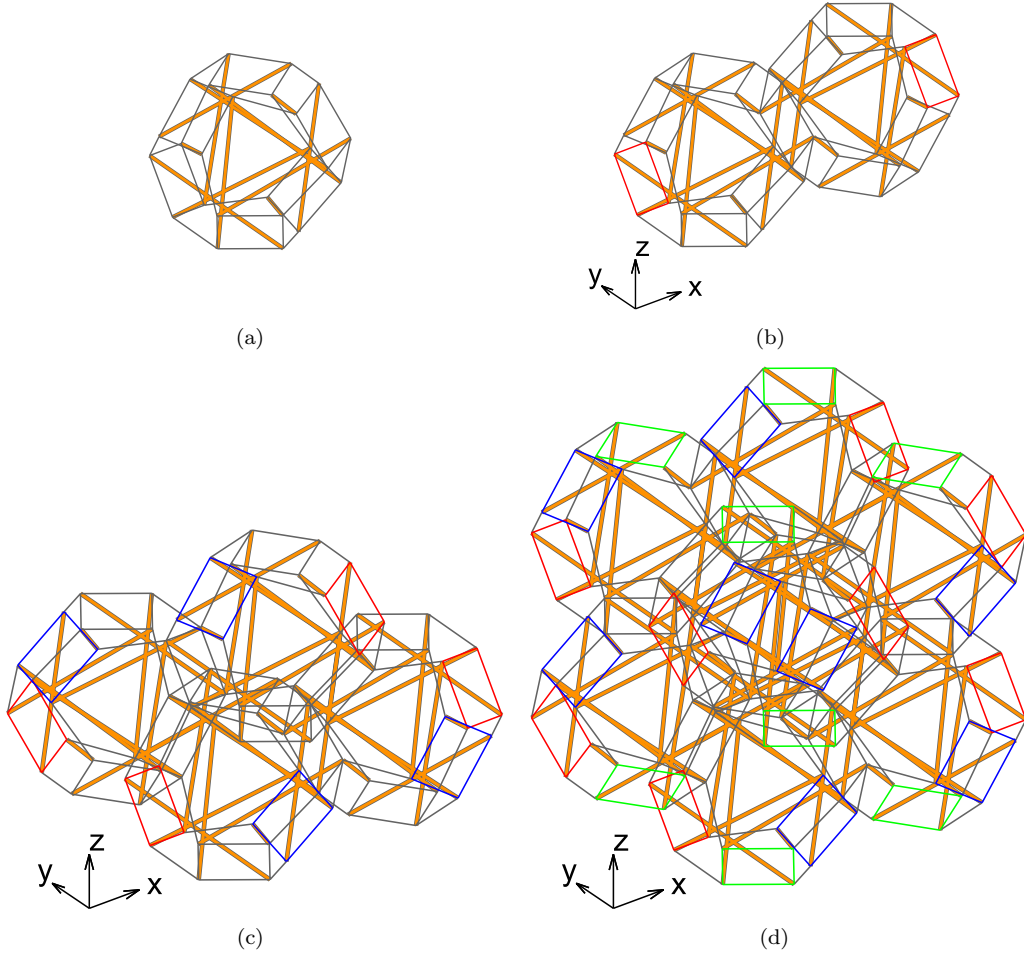


Figure 1: (a) Tensegrity sphere with a truncated octahedron geometry. Unit cells for a tensegrity beam (b), plate (c) and solid (d), obtained by successive reflection operations to get translation symmetry and preserve discontinuity in compression. After [1].

we conduct a dispersion analysis on a single unit cell of the periodic tensegrity lattice. Periodic boundary conditions are imposed relating the displacements on the nodes at the two opposite square facets at the boundary of the unit cell, illustrated by the same color in Fig. 1.

All the calculations in this letter are done with material properties for bars and cables corresponding to titanium with density 4480 kg/m^3 and Young's modulus 100 GPa . The bar and cable diameters are taken to be 2.3 cm and 1.15 cm , respectively, while the length of the canonical unit cell is 1.26 m . The frequencies are normalized by a reference frequency $\omega_r = c_0/a$, where a is the magnitude of the lattice vector and $c_0 = \sqrt{E/\rho}$ is the longitudinal wave speed in the bulk material comprising the tensegrity structure. The non-dimensional frequency is thus given by $\Omega = \omega/\omega_r$. This choice of normalization ensures that the dispersion diagrams are valid for tensegrity lattice made of any linear elastic material and over any length scale where linear elasticity assumptions are valid, provided that the relative geometric dimensions of the cable and bar diameters with respect to the unit cell length a are the same. Although we study only one geometric configuration, we believe these results are representative of a wide range of cable and bar dimensions.

3. Dispersion analysis of 1D, 2D and 3D tensegrity media

The dispersion analyses of tensegrity based beams, plates and solids are presented for different levels of cable prestrain λ . We examine the low frequency (long wavelength) propagation of acoustic modes through the lattice and contrast their behavior with waves in conventional bulk media. Note that due to the presence of free surfaces (faces) in tensegrity beams and plates, the strain in the various cables (and thus bars), lying in the interior or on a free surface, may be different in the reference configuration. As the prestrain increases (decrease in λ), the bars experience increasing compression and eventually all the bars buckle. To illustrate qualitative differences between the cases when the bars are unbuckled and buckled in the equilibrium configuration, we present dispersion diagrams for two prestrain levels λ : one where bars are unbuckled ($\lambda = \lambda_u = 0.993$) and another where all the bars buckle ($\lambda = \lambda_b = 0.988$). It is worth emphasizing that a post-buckled dynamic analysis is possible

due to the unique ability of our lattice to be stable and support loads even after the bars buckle [1].

Let us make a technical remark on the mechanics of a buckled bar. In each bar, there is a $U(1)$ gauge freedom in the choice of the buckling plane, i.e., the transverse displacement of a buckled bar can be in any direction orthogonal to its axis. Let us consider a local coordinate system with the x -axis along the centerline and the y -axis along the transverse displacement direction. The quasistatic response of the post-buckled beam (and hence lattice) is gauge independent as the transverse (y direction) force (and stiffness) in the plane of buckling is the same as that normal to this plane (i.e., along z). However, under dynamic excitation, this gauge invariance is broken as the force in the transverse direction (y) is nonzero while it is zero in the out of plane (z) direction. Thus our post-buckled results will depend on the choice of our gauge for the buckled configuration of each bar. Our numerical simulations showed that this choice does not significantly influence the dispersion results at low frequencies and long wavelengths (wavevector $\kappa \rightarrow \mathbf{0}$). At large wavevectors κ and high frequencies, there are small variations in the dispersion behavior. In this work, we choose a gauge such that the beams always buckle in the local xy plane, with x being along the direction \mathbf{v} of the line joining the two end points and y given by the unit vector along $\mathbf{e}_3 \times \mathbf{v}$, with \mathbf{e}_3 being the unit vector along the global z direction.

3.1. 1D lattice: Tensegrity beams

The tensegrity beam is obtained by tessellating the unit cell in Fig. 1(b) along the x direction. Its unit cell comprises of 24 bars and 68 cables. Figure 2 displays its dispersion diagram for the two prestrain levels discussed above. For a prestrain λ_u (Fig. 2(a)), under which the bars are in compression, while all the cables are in tension, there are four acoustic modes: two coincident bending modes, an axial mode and a torsional mode, in increasing order of frequency. The coinciding of the two bending modes follows from their orthogonality and from the C_4 symmetry of the beam unit cell about its axis.

Figure 2(b) displays the dispersion diagram for a cables prestrain λ_b , where the bars are buckled. In addition to the four acoustic modes, it has a collection of 24 flat modes at low frequencies ($\Omega \sim 0.02 - 0.04$). The buckling of the bar introduces these low frequency wave modes and these modes are defined as soft modes. There are also 24 zero

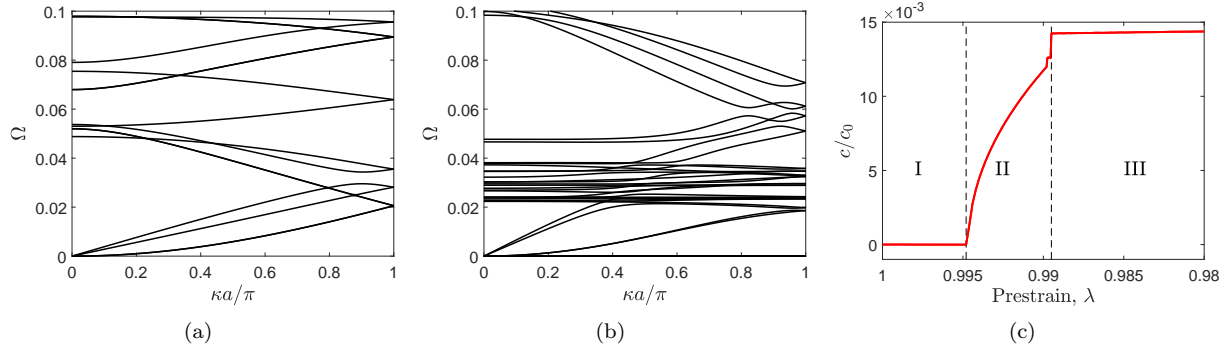


Figure 2: Tensegrity beam dispersion diagram for bars (a) prebuckled (λ_u) and (b) post-buckled (λ_b), with an axial, a torsional and two bending modes at low Ω . The flat branches are due to soft modes in the buckled configuration. (c) Effect of prestrain on the wave speed of various waves showing two sharp transitions: when the lattice becomes stiff and when the bars buckle.

frequency modes ($\Omega = 0$) in the dispersion diagram. Each buckled bar contributes to a zero energy mode and a soft mode and these additional modes arise as a consequence of buckling in a single bar. A buckled bar can freely rotate about the line joining its ends since the pin joints do not offer any resistance. This rotation about the axis is a zero energy (floppy) mode and leads to the zero frequency branch in the dispersion diagram. The flat modes at finite frequency in Fig. 2(b) arise from the interaction of the cables with the axial deformation of the buckled bars. Since the axial stiffness of a buckled beam is significantly lower, this mode has a low frequency.

Having demonstrated qualitative differences between tensegrity beams with bars in the pre- and post-buckled configurations, let us now quantify this difference by analyzing the wave speeds in the long wavelength regime ($\kappa \rightarrow 0$). These are computed by using the approximation $c = \partial\Omega/\partial\kappa \approx \Delta\Omega/\Delta\kappa = \Omega/\kappa$ at a κ close to zero. The wave speeds are normalized by $c_0 = \sqrt{E/\rho}$. Figure 2(c) displays the axial acoustic mode wave speed as a function of the prestrain level λ . Three distinct regimes are observed: at low prestrains (labeled I in the figure), the wave speeds are zero. There are floppy modes (mechanisms) which result in these zero energy (or zero frequency) modes. At moderate prestrain values (labeled II in the figure), the wave speeds increase monotonically from zero. The bending wave speed is also nonzero, but it is small compared to the axial wave speed. At a prestrain level $\lambda = 0.9898$, 8 bars in the unit cell buckle, resulting in a jump in the wave speed. At $\lambda = 0.9895$, the remaining 16 bars buckle, resulting in a second, larger jump in wave speed. Finally, as the prestrain

increases further, the axial wave speed remains at a near constant value. The transitions between the stages are analogous to phase transitions in condensed matter systems [26]. These results illustrate how the wave speeds of our tensegrity-based beams can be varied over a wide range by varying the cable prestrain.

3.2. 2D lattice: Tensegrity plates

We now turn attention to analyzing the dynamic behavior of tensegrity plate lattices obtained by tesselating the unit cell in Fig. 1(c) along x and y directions. We present the dispersion diagrams for two levels of cable prestrain (λ_u and λ_b) along the corners of the irreducible Brillouin zone (IBZ). The IBZ corners span the path $\Gamma M X \Gamma$ with $\Gamma = (0, 0)$, $M = (\pi/a, 0)$ and $X = (\pi/a, \pi/a)$. Figure 3(a) displays the low frequency modes for the case where the cable prestrain is set to λ_u . It has three acoustic modes, analogous to that observed in a plate made of a continuous solid.

The first mode is analogous to an A_0 Lamb mode in a conventional plate and is antisymmetric about the plate midplane. The second acoustic mode is symmetric about the plate midplane, analogous to the S_0 Lamb wavemode while the third acoustic mode has an inplane shear mode shape, analogous to SH modes in plates. Similar to a conventional plate, the A_0 -like mode has the lowest wave speed, followed by the S_0 -like mode and the in-plane shear mode. Figure 3(b) displays the dispersion diagram for the lattice with cable prestrain set to λ_b . Similar to the 1D case, 48 flat modes corresponding to zero energy modes are present at $\Omega = 0$ and around $\Omega = 0.02$. The acoustic mode shapes in the post-

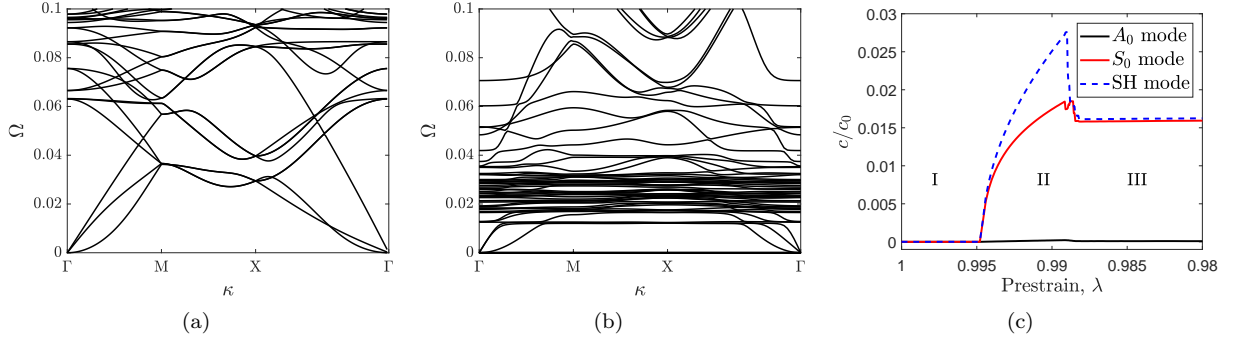


Figure 3: Tensegrity plate dispersion diagram along the IBZ corners for (a) prebuckled bars (λ_u) and (b) post-buckled bars ($\lambda = 0.988$), showing a bending mode, two coincident S_0 modes and a transverse shear (SH) mode. The additional lines in (b) are due to soft modes. (c) Wave speed with prestrain for the various wave modes having two sharp transitions.

buckled case are identical to the presented case of a prestrain level where the bars are unbuckled.

Let us analyze the effect of cable prestrain on the wave speeds to quantify the difference in behavior when the bars are pre- and post-buckled. Figure 3(c) displays the variation of the acoustic mode wave speeds with prestrain parameter λ along the lattice unit vector (x or y) directions. Similar to the 1D case, three distinct regimes are observed. At low prestrains (labeled I in the figure), the wave speeds are zero, while it monotonically increases from zero at moderate prestrains. This range (labeled II in the figure) corresponds to the bars being unbuckled. As the bars begin to buckle with increasing prestrain, the S_0 and SH mode wave speeds decrease to an almost constant value. The bars begin to buckle in sets of 4 or 8 starting from a prestrain $\lambda = 0.9892$, in six stages until a prestrain level $\lambda = 0.9882$, when all the bars are buckled. These sets of buckling correspond to small jumps in the S_0 mode wave speed around $\lambda = 0.98$ in Fig. 3(c).

Let us now look at the wave speeds in all directions to understand anisotropy in the lattice response to a point excitation. For each wave-vector $\boldsymbol{\kappa} = (\kappa_x, \kappa_y)$ near $\mathbf{0}$ and mode m with frequency Ω_m , we compute the group velocity $\mathbf{c} = (c_{g,x}, c_{g,y})$ in each direction by approximating $\partial\Omega_m/\partial\boldsymbol{\kappa}$, i.e., the components of the group velocity are $c_{g,x} = \Omega_m/\kappa_x$ and $c_{g,y} = \Omega_m/\kappa_y$. The variation with direction is obtained by simply setting $\boldsymbol{\kappa} = \kappa(\cos\theta, \sin\theta)$ and spanning θ in $[0, 2\pi]$. κ is chosen to be sufficiently small to get the wave speeds at low frequency.

Figure 4 displays the directional variation of wave speeds of the three acoustic modes for the two prestrain levels, λ_u and λ_b . These two cases are rep-

resentative of the behavior in the second and third stages in Fig. 3(c). Figure 4(a) displays the group velocity components for the A_0 or flexural mode for both the prestrain cases. The group velocity variation exhibits a four fold symmetry, consistent with the D_4 lattice symmetry and becomes more isotropic as the bars become buckled (λ_b). Note that the group velocity decreases linearly to zero with decreasing Ω , since the frequency scales as $\Omega \sim |\kappa|^2$ for the flexural mode. Hence, this group velocity plot illustrates only the shape of the variation with direction as $\kappa \rightarrow 0$ (the magnitude of c_g is meaningless here).

Figure 4(b) displays the group velocity variation with direction for the S_0 and SH modes at a prestrain level λ_u . The S_0 mode exhibits strong anisotropy and the group velocity is high along the lattice directions. In contrast the SH mode is relatively isotropic and its maximum wave speed is along the diagonal directions. Finally, Fig. 4(c) displays the group velocity contours for the lattice with prestrain level λ_b . It is qualitatively similar to the unbuckled case, with a reduced anisotropy in the S_0 mode. In both the cases, the S_0 waves travel slower than the SH waves in all directions, similar to the typical response of a plate made of conventional solids.

3.3. 3D lattice: Tensegrity solids

Let us now analyze the dynamic behavior of tensegrity solids obtained by tessellating its unit cell (Fig 1(d)) along x , y and z directions. The lattice unit cell has cubic symmetry as all the cables have identical prestrain [27]. The first Brillouin zone is a cube and the irreducible Brillouin zone is a tetrahedron [28], illustrated in Fig. 5(c). Figure 5(a)

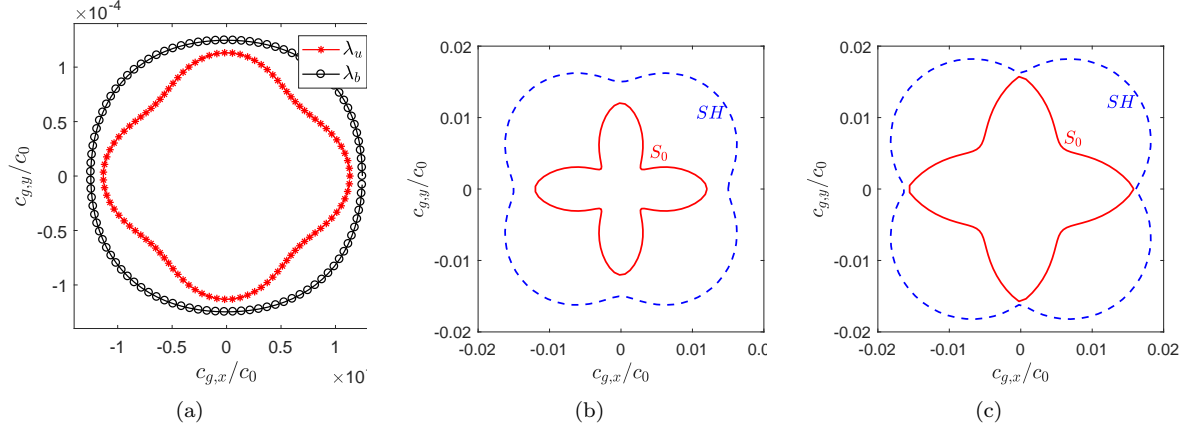


Figure 4: Wave speed variation with direction near $\kappa = 0$ for two prestrain levels. (a) Flexural or A_0 mode. S_0 and SH modes for bars in (b) pre-buckled and (c) post-buckled configuration.

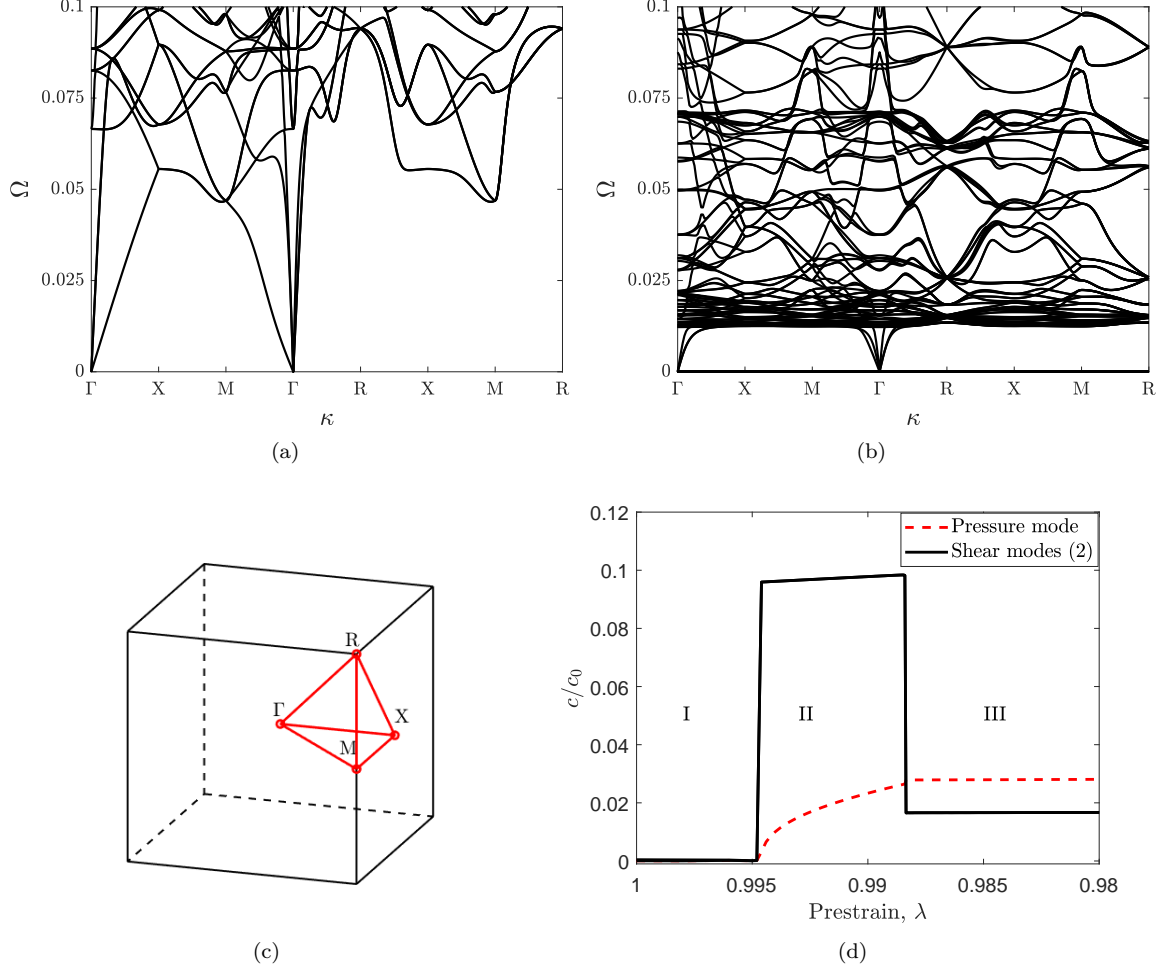


Figure 5: Tensegrity solid dispersion diagram along the corners of the IBZ (shown in (c)) for (a) prebuckled bars and (b) post-buckled bars, both having one pressure mode and two shear modes at low Ω . The flat curves in (b) again correspond to soft modes. (d) Effect of prestrain on the wave speeds. Shear waves travel faster than pressure waves in the prebuckled configuration, while this gets reversed in the post-buckled configuration.

displays the first few modes of the dispersion diagram for a prestrain λ_u . There are three acoustic modes: a pressure mode and two shear modes. The shear modes are doubly degenerate along the ΓX direction as a consequence of the cubic symmetry of the lattice [27]. Contrary to most solids [29], the two shear waves have a higher group velocity than the longitudinal wave in all directions. The contour diagrams of group velocity variation presented later in this section illuminate this behavior clearly. Figure 5(b) displays the dispersion diagram at low frequencies when the cables are subjected to a prestrain λ_b , where the bars are buckled in the equilibrium configuration. Similar to the dispersion diagrams of tensegrity beams and plates, there are 96 zero frequency modes and an equal number of soft modes. The acoustic shear mode gets hybridized with these soft modes and it does not propagate in these band of frequencies. These flat bands effectively act as stop bands only for shear waves.

Figure 5(d) displays the variation of wave speeds for the long wavelength acoustic modes along the x -direction as the cable prestrain is varied. Again, three distinct regions are observed, with sharp jumps between them, analogous to phase transitions in solids. As the prestrain parameter λ decreases below 0.995, the shear and pressure wave speeds jump from zero to a finite value. They remain almost constant for the entire range of prestrain where the bars are prebuckled. The shear wave speeds are higher than the pressure wave speed. As the cable prestrain increases, the bars buckle at $\lambda = 0.9885$ and the wave speed decreases. Note that all the bars are under the same compression in the reference configuration due to symmetry and they all buckle simultaneously. When the bars buckle, the pressure wave speed becomes higher than the shear wave speed, similar to the behavior of conventional solids [29]

To gain insight on the directional variation of the acoustic mode wave speeds in the lattice, we examine the dispersion surfaces in the long wavelength limit. A similar procedure to that used for plates is employed here for computing this directional variation. We span the directions associated with the set of normal vectors to a unit sphere by setting $(\kappa_x, \kappa_y, \kappa_z) = \kappa(\cos \phi \sin \theta, \sin \phi \sin \theta, \cos \theta)$. Here θ and ϕ span $[0, \pi]$ and $[0, 2\pi]$, respectively, and κ is sufficiently small to get the long wavelength non-dispersive wave speeds. Figure 6 displays the variation with direction for the three acoustic modes,

with both the color and the magnitude in the radial direction denoting the wave speed. When the cable prestrain level is λ_u , the pressure wave speed is higher along the long (example: $[1, 1, 1]$) diagonal directions (Fig. 6(a)). The two shear modes (Fig. 6(c),(e)) in the prebuckled configuration have a directional variation close to an isotropic sphere. The degeneracy in the two shear acoustic modes in Fig. 5 is along the high symmetry directions (ΓX , ΓR and ΓM) only, as evident from the distinct shapes of their dispersion surfaces (Fig. 6(e,f)). Note from the range of the color bars that the lowest shear wave speed is higher than the maximum pressure wave speed. Thus, both shear modes are faster than the pressure mode in all directions. Similar trends have recently been observed in dilational metamaterials in [30].

Figures 6(b,d,f) display the group velocity variation with direction when the cable prestrain is λ_b . The pressure wave speed increases along the coordinate directions and decreases along the diagonal $[\pm 1, \pm 1, \pm 1]$ directions. Note also from the range of the colorbar that the mean wave speed value is significantly lower than the unbuckled case. Similarly, the shear wave speeds also decrease by a factor of about 5 although the contour shape remains qualitatively similar. The pressure waves travel faster than the shear waves along the coordinate directions, while the shear waves travel faster along the long diagonal directions, illustrating the unique dynamic properties of our tensegrity solid.

The three key aspects of dispersion analysis in tensegrity solids: faster shear than pressure waves at low prestrains, flipping to conventional behavior with faster pressure waves and the flat bands acting as stopbands for shear waves are verified by numerical simulations on finite lattices. Details are presented in the accompanying Supplementary Materials. Thus the dynamic response of our tensegrity solids can change significantly as the bars buckle due to the cable prestrain.

4. Conclusions

Tensegrity-based periodic media offer unique opportunities for tunable wave propagation by varying the cable prestrain. In this letter, we presented a linear wave propagation analysis of tensegrity-based beams, plates and solids. Dispersion analysis is used to investigate the dynamic response of these structural units and it shows a significant change in their long wavelength acoustic mode wave speeds

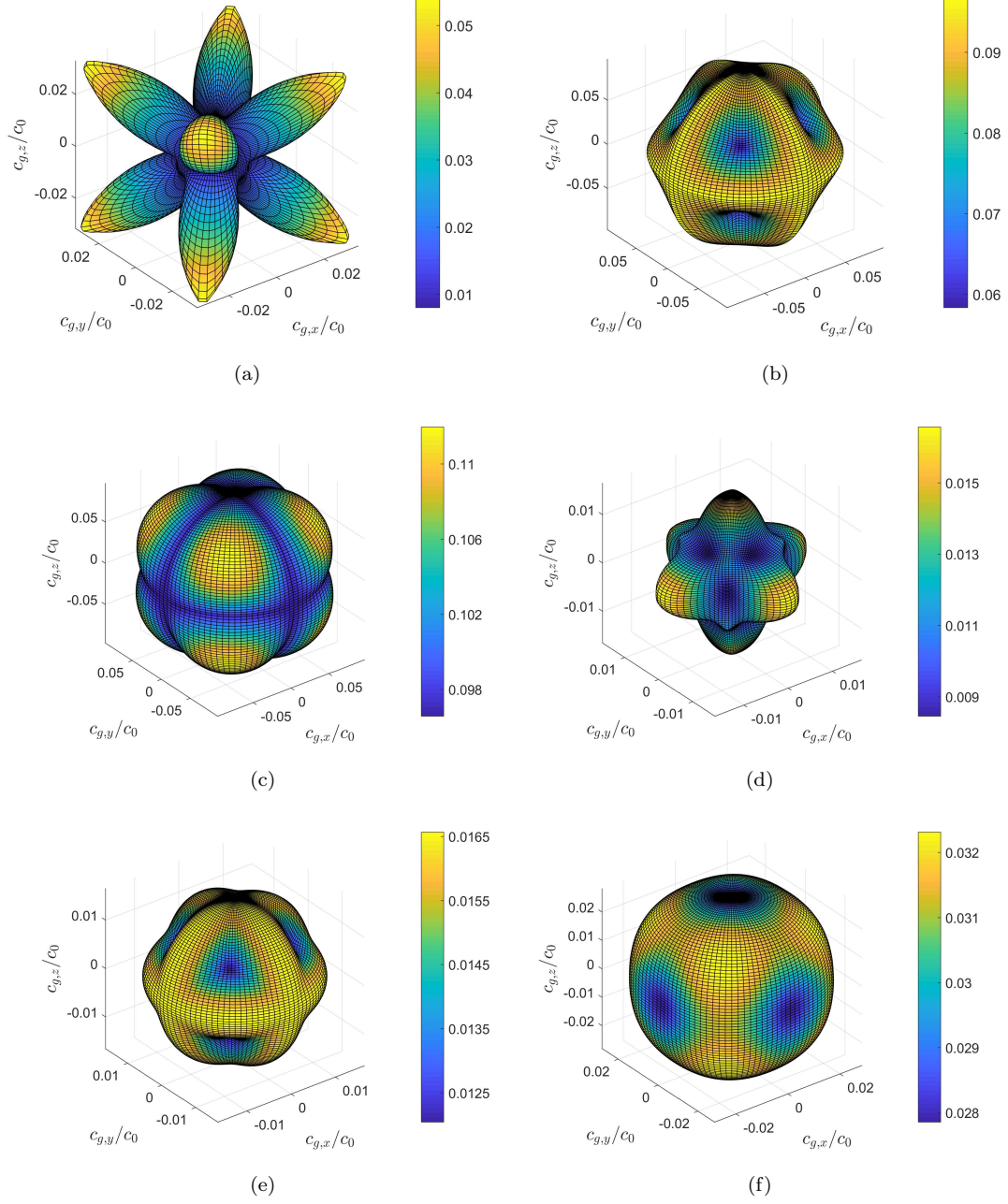


Figure 6: Dispersion surface of the tensegrity solid near $\kappa = 0$ for the prebuckled (a,c,e) and post-buckled (b,d,f) configurations. (a) and (b) show pressure modes while the remaining plots show the two shear modes for each configuration. The behavior is anisotropic and changes as the bars in the unit cell buckle under prestrain.

as a function of the cable prestrain. Three distinct stages are identified: at low prestrain levels, the wave speeds are zero as the structure has zero stiffness; at moderate prestrain levels when the bars are under compression but not buckled, the wave speed is nonzero and finally, at prestrain levels where the bars have buckled, the wave speed is distinct. Sharp transitions in wave speeds are observed between the three stages, analogous to phase transitions in a solid. Our tensegrity solids are observed to support an unusual dynamic property of faster shear waves than pressure waves in all directions in the second stage. In the post-buckled regime, additional zero frequency modes and soft modes having flat dispersion bands are observed in all the three structural units. A collection of these flat bands essentially acts as stop bands for shear excitations and opens new avenues in achieving low frequency bandgaps. In summary, the unique post-buckling stability of these lattices allows for exploiting these sharp effective phase transitions to get qualitatively distinct dynamic behaviors as the bars buckle.

References

- [1] J.J. Rimoli and R.K. Pal. Mechanical response of 3-dimensional tensegrity lattices. *Composites Part B: Engineering*, 115:30–42, 2017.
- [2] M.I. Hussein, M.J. Leamy, and M. Ruzzene. Dynamics of phononic materials and structures: Historical origins, recent progress, and future outlook. *Applied Mechanics Reviews*, 66(4):040802, 2014.
- [3] J. Christensen, M. Kadic, O. Kraft, and M. Wegener. Vibrant times for mechanical metamaterials. *Mrs Communications*, 5(3):453–462, 2015.
- [4] T. Bückmann, M. Thiel, M. Kadic, R. Schittny, and M. Wegener. An elasto-mechanical unfeelability cloak made of pentamode metamaterials. *Nature communications*, 5:4130, 2014.
- [5] Z. Wang, Y. Chu, C. Cai, G. Liu, and M.R. Wang. Composite pentamode metamaterials with low frequency locally resonant characteristics. *Journal of Applied Physics*, 122(2):025114, 2017.
- [6] S. Babae, J. Shim, J.C. Weaver, E.R. Chen, N. Patel, and K. Bertoldi. 3d soft metamaterials with negative poisson’s ratio. *Advanced Materials*, 25(36):5044–5049, 2013.
- [7] R.S. Lakes. Negative-poisson’s-ratio materials: Auxetic solids. *Annual Review of Materials Research*, (0), 2017.
- [8] M. Ruzzene, F. Scarpa, and F. Soranna. Wave beaming effects in two-dimensional cellular structures. *Smart materials and structures*, 12(3):363, 2003.
- [9] D. Tallarico, N.V. Movchan, A.B. Movchan, and D.J. Colquitt. Tilted resonators in a triangular elastic lattice: chirality, bloch waves and negative refraction. *Journal of the Mechanics and Physics of Solids*, 103:236–256, 2017.
- [10] K. Bertoldi. Harnessing instabilities to design tunable architected cellular materials. *Annual Review of Materials Research*, (0), 2017.
- [11] R.K. Pal, J. Rimoli, and M. Ruzzene. Effect of large deformation pre-loads on the wave properties of hexagonal lattices. *Smart Materials and Structures*, 25(5):054010, 2016.
- [12] Evgueni T Filipov, Tomohiro Tachi, and Glaucio H Paulino. Origami tubes assembled into stiff, yet reconfigurable structures and metamaterials. *Proceedings of the National Academy of Sciences*, 112(40):12321–12326, 2015.
- [13] Ke Liu, Jiangtao Wu, Glaucio H Paulino, and H Jerry Qi. Programmable deployment of tensegrity structures by stimulus-responsive polymers. *Scientific Reports*, 7, 2017.
- [14] B.F. Richard. Tensile-integrity structures, November 13 1962. US Patent 3,063,521.
- [15] A. Pugh. *An introduction to tensegrity*. Univ of California Press, 1976.
- [16] R.E. Skelton and M.C. de Oliveira. *Tensegrity systems*, volume 1. Springer, 2009.
- [17] A Amendola, A Krushynska, C Daraio, NM Pugno, and F Fraternali. Tuning frequency band gaps of tensegrity metamaterials with local and global prestress. *arXiv preprint arXiv:1803.03472*, 2018.
- [18] C Paul, JW Roberts, H Lipson, and FJV Cuevas. Gait production in a tensegrity based robot. In *Advanced Robotics, 2005. ICAR’05. Proceedings., 12th International Conference on*, pages 216–222. IEEE, 2005.
- [19] J.J. Rimoli. A reduced-order model for the dynamic and post-buckling behavior of tensegrity structures. *Mechanics of Materials*, 2017.
- [20] F. Fraternali, G. Carpentieri, A. Amendola, R.E. Skelton, and V.F. Nesterenko. Multiscale tunability of solitary wave dynamics in tensegrity metamaterials. *Applied Physics Letters*, 105(20):201903, 2014.
- [21] R. Connelly and M. Terrell. Globally rigid symmetric tensegrities. *Structural Topology* 1995 núm 21, 1995.
- [22] N.B. Kahla and K. Kebiche. Nonlinear elastoplastic analysis of tensegrity systems. *Engineering Structures*, 22(11):1552–1566, 2000.
- [23] L. Zhang, M.K. Lu, HW Zhang, and B Yan. Geometrically nonlinear elasto-plastic analysis of clustered tensegrity based on the co-rotational approach. *International Journal of Mechanical Sciences*, 93:154–165, 2015.
- [24] N. Vassart and R. Motro. Multiparametered formfinding method: application to tensegrity systems. *International Journal of Space Structures*, 14(2):147–154, 1999.
- [25] R.K. Pal, M. Ruzzene, and J.J. Rimoli. A continuum model for nonlinear lattices under large deformations. *International Journal of Solids and Structures*, 96:300–319, 2016.
- [26] G Jaeger. The ehrenfest classification of phase transitions: introduction and evolution. *Archive for history of exact sciences*, 53(1):51–81, 1998.
- [27] H. Salahshoor, R.K. Pal, and J.J. Rimoli. Phase transition in tensegrity lattices by varying cable prestrain. *arXiv*, 2017.
- [28] C. Bradley and A. Cracknell. *The mathematical theory of symmetry in solids: representation theory for point groups and space groups*. Oxford University Press, 2010.
- [29] J. Achenbach. *Wave propagation in elastic solids*, volume 16. Elsevier, 2012.

- [30] T. Bückmann, R. Schittny, M. Thiel, M. Kadic, G.W. Milton, and M. Wegener. On three-dimensional dilational elastic metamaterials. *New Journal of Physics*, 16(3):033032, 2014.